Journal of the Physical Society of Japan
Vol. 76, No. 9, September, 2007, 094707

Superconducting Transitions in Wire Network under Spatially Modulated Magnetic Field

Hirotaka SANO*, Akira ENDO, Shingo KATSUMOTO, and Yasuhiro IYE

Institute for Solid State Physics, University of Tokyo, 5-1-5 Kashiwanoha, Kashiwa, Chiba 277-8581

(Received May 14, 2007; accepted July 5, 2007; published August 27, 2007)

Superconducting wire network subjected to a uniform and a checkerboard-patterned magnetic field is investigated. The checkerboard field is created by an array of ferromagnetic dots placed on top of the superconducting network. Measurements of the current–voltage (I–V) characteristics have revealed the canonical Kosterlitz–Thouless–Berezinskii (KTB) transition at zero magnetic field. The superconducting transition at $\alpha = 1/2$ (α being the frustration parameter) is studied in detail, and compared with the theoretical predictions on the fully frustrated XY model which has a double degeneracy in the ground state vortex configuration. The I–V characteristics for $\alpha = 1/2$ is consistent with the scenario of kink–antikink unbinding at antiphase domain boundaries first proposed by Korshunov [Phys. Rev. Lett. **88** (2002) 167007]. Introduction of the checkerboard field with amplitude β to the $\alpha = 1/2$ case lifts the double degeneracy. The effect of non-zero β on the nature of superconducting transition at $\alpha = 1/2$ is consistent with this picture. The KTB transition is restored at $\beta = 1/2$.

KEYWORDS: superconducting wire network, magnetic field modulation, Little–Parks oscillation, FFXY model
DOI: 10.1143/JPSJ.76.094707

1. Introduction

The nature of phase transition in artificially structured superconducting systems such as superconducting wire network (SWN) and Josephson junction array (JJA) has been the subject of intensive studies both experimental and theoretical.[1)] The phase transition of a superconductor can be described by the complex order parameter $\psi = |\psi| \exp(i\theta)$. Corresponding to the two (amplitude and phase) degrees of freedom, the phase transitions in these systems can occur in two steps. Upon cooling, the amplitude $|\psi|$ of the superconducting order parameter grows first around the mean field transition temperature T_{MF} of the superconducting material. Subsequent ordering of the phase θ of the order parameter over the entire system takes place at $T_c < T_{MF}$. It is the latter global phase ordering process in artificially structured superconducting systems that has attracted much interest, as it can be mapped onto the ordering problem of an XY spin system. Above T_c, motion of vortices created by thermal fluctuations gives rise to dissipation and hence non-zero resistance. Disappearance of free vortices at T_c leads to vanishing linear resistance. In this sense, this transition is regarded as the true superconducting transition of the system.

For the case of a two-dimensional (2D) network in the absence of magnetic field, the ground state is a "ferromagnetic" state in which the order parameters (XY spins) are uniformly aligned over the entire system. The transition from the high temperature phase-disordered state to the low temperature ordered state is theoretically predicted and experimentally verified to be the so-called Kosterlitz–Thouless–Berezinskii (KTB) type.[1–3)]

An external magnetic field perpendicular to the 2D plane introduces an interesting twist to the problem. In the presence of a vector potential $\mathbf{A}$, the Aharonov–Bohm phase is added to the phase difference between the sites i and j.

$$\Delta\theta_{ij} = \theta_j - \theta_i - A_{ij}, \tag{1}$$

$$A_{ij} = \frac{2e}{\hbar}\int_i^j \mathbf{A}(\mathbf{r}) \cdot \mathrm{d}\mathbf{r}. \tag{2}$$

Thus the external field introduces "frustration" to the phase ordering. The relevant parameter is $\alpha \equiv \Phi/\Phi_0$ which is called frustration parameter or vortex filling. It represents the average number of flux quanta per plaquette. Here, $\Phi_0 = h/2e$ is the superconducting flux quantum and Φ is the average external flux piercing the unit cell. The sum of A_{ij} over any unit loop must satisfy

$$\sum_{\text{loop}} A_{ij} = 2\pi\alpha. \tag{3}$$

The frustration affects various aspects of superconducting behavior of SWN. (Although we refer only to SWN hereafter, much of the physics involved is also relevant to JJA.) The mean field transition temperature T_{MF} shows periodic variations versus α, known as the Little–Parks oscillations (LPO). The $T_{MF}(\alpha)$ curve shows a series of cusp-like peaks at integer values of α and substructures (smaller cusps) at simple fractional values.[4–6)] The substructures within each period of LPO have an interesting one-to-one correspondence with the so-called Hofstadter butterfly,[7)] i.e., energy spectra of a 2D tight-binding model under a perpendicular magnetic field. According to the correspondence, the relative change in T_{MF} is given by

$$\frac{\Delta T_{MF}(\alpha)}{T_{MF}(0)} = -\frac{\xi^2(0)}{s^2}\arccos^2\left(\frac{\varepsilon(\alpha)}{4}\right), \tag{4}$$

where $\xi(0)$ is the superconducting coherence length at zero temperature, s is the lattice constant, and $\varepsilon(\alpha)$ represents the maximum eigenvalue of the Hofstadter spectrum for each value of α (normalized by the band width). In other words, $\Delta T_{MF}(\alpha)$ is isomorphic to the spectral edge of the Hofstadter butterfly. The subpeaks in the $\Delta T_{MF}(\alpha)$ curve at simple fractional α reflect stable vortex configurations at such

*E-mail: h-sano@issp.u-tokyo.ac.jp

fillings. The vortex configuration at $\alpha = 1/2$ for a square SWN, for instance, is that of checkerboard pattern.

Introduction of frustration is of great interest in the context of the XY model. Experimentally, the superconducting transition under frustration has been studied by various researchers.[2,3,8,9] In fact, SWNs are regarded as suitable experimental systems for study of critical phenomena in frustrated XY models, since the degree of frustration can be tuned by the applied magnetic field. However it is fair to say that the nature of phase transition for non-zero α is still not fully elucidated, in comparison to the well-established KTB mechanism for the unfrustrated case. In particular, the half-filled ($\alpha = 1/2$) case, which is mapped to the so-called fully frustrated XY (FFXY) model, attracts much interest.[10] The characteristic feature of the FFXY model lies in the double degeneracy of ground state vortex configuration. It is the extra degree of freedom associated with this degeneracy that renders the phase transition of the FFXY system complicated and intriguing.

Most of the experiments on SWN to date were conducted by use of uniform external magnetic field. Adding a spatially modulated magnetic field extends the parameter space. In a series of preceding studies,[11–13] we fabricated hybrid superconductor/ferromagnet systems in which a SWN was decorated by an array of ferromagnetic dots, whose role was to impose a checkerboard-patterned magnetic field onto the SWN. We investigated the evolution of LPO pattern as a function of both the uniform and the modulated magnetic fields and demonstrated that the behavior agrees very well with the evolution of the corresponding Hofstadter problem. In this work, we extend the study to explore the details of the superconducting transition. In particular, we focus on the transition at $\alpha = 1/2$ and investigate how it is affected by the checkerboard field. In the context of the FFXY model at $\alpha = 1/2$, introduction of a checkerboard-patterned external field lifts the double degeneracy of the vortex configuration and thereby alters the aforementioned extra degree of freedom. The experimental results are compared with the theoretically predicted behavior of the FFXY model.

This paper is organized as follows: Section 2 describes the experimental method of the present work. The experimental results are presented in §3, and discussed in the context of the FFXY model in §4. Section 5 gives a few concluding remarks.

2. Experimental Method

Figure 1(a) shows a scanning electron micrograph of the SWN sample used in this study. The square network pattern with $s = 500$ nm was drawn on a resist-coated Si substrate by electron beam lithography. Aluminum wire network was then fabricated by vacuum evaporation followed by lift-off process. The network consisted of 300×300 squares formed by 40 nm thick and 50 nm wide Al wires. Six leads were attached to the Al-SWN as shown in Fig. 1(b). The electrode pads were made of Ti/Au. Current was passed between the electrodes 2 and 5 which covered the whole length of the sides of the SWN to ensure uniform current injection. Voltage between the electrodes 1 and 6 was recorded, while that on the other side of the SWN (3 and 4) was used for check against nonuniformity of superconducting transition. Figure 1(a) also shows a regular array of ferromagnetic Co dots of area $\sim 150 \times 350\,\mathrm{nm}^2$ and thickness ~ 80 nm placed on top of the Al SWN. The Co dot was placed on every other bond segment in the y-direction. Figure 1(c) is a schematic crosssectional view, showing the Co dots overbridging the Al wire. The Al SWN and the Co dots were separated by a 30 nm thick layer of Ge, so that no pair-breaking effect was involved and the sole effect of the ferromagnetic dots was due to the stray field emanating from them. When an in-plane magnetic field of sufficient strength (typically 500 mT) was applied as shown in Fig. 1(c), the Co dots were fully magnetized and the stray field from the Co dots created a spatially modulated magnetic field. The Co dot arrangement shown in Fig. 1(a) generated a checkerboard flux pattern, i.e., alternating flux piercing the plaquettes of the SWN. The amplitude of the checkerboard flux pattern was controlled by changing the azimuthal angle φ of the in-plane (magnetizing) field from the y-axis, defined in Fig. 1(a). Starting from $\varphi = 0$, the magnetization of the Co dots is aligned to the y-axis, so that the total flux piercing each unit cell cancels to zero. As φ is increased (i.e., by tilting the in-plane field away from the y-axis), the stray field from a Co dot becomes unequal for two adjacent unit cells, resulting in a staggered flux pattern. The amplitude of the checkerboard-pattern flux, called β hereafter, is defined in the same unit as α, i.e., flux per plaquette in the unit of Φ_0. For a saturating in-plane magnetic field, the amplitude β is proportional to $\sin\varphi$.

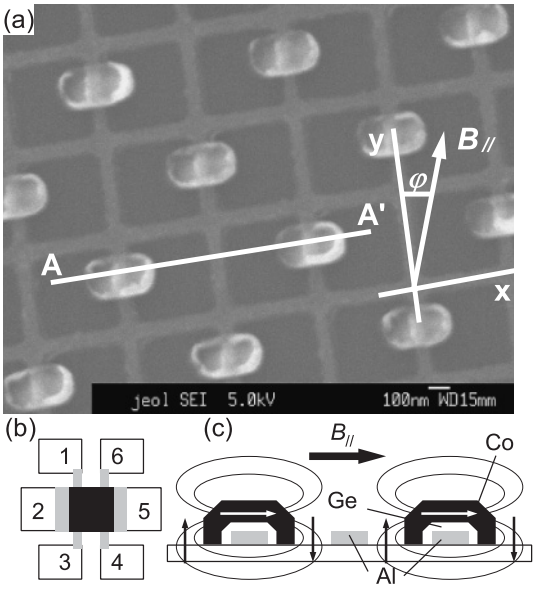

Fig. 1. (a) Scanning electron microscope image of the Al network decorated with an array of Co dots. The x and y axes and φ are indicated. (b) The electrode configuration. Al SWN with Co dots (black square) was connected to the Ti/Au electrode pads 1–6 by Al film (gray part). (c) Schematic drawing of a crosssection of A–A′ indicated in (a). The Al wire and the overbridging Co dot are separated from each other by an intervening Ge layer. The stray magnetic field emanating from the Co dots creates a staggered flux pattern.

We used a cross-coil magnet system, consisting of a horizontal split coil and a vertical solenoid, to independently control α and β. The sample was mounted horizontal so that α was controlled by the vertical field generated by the solenoid, while β was controlled by changing the azimuthal angle φ of the horizontal field by rotating the sample in the

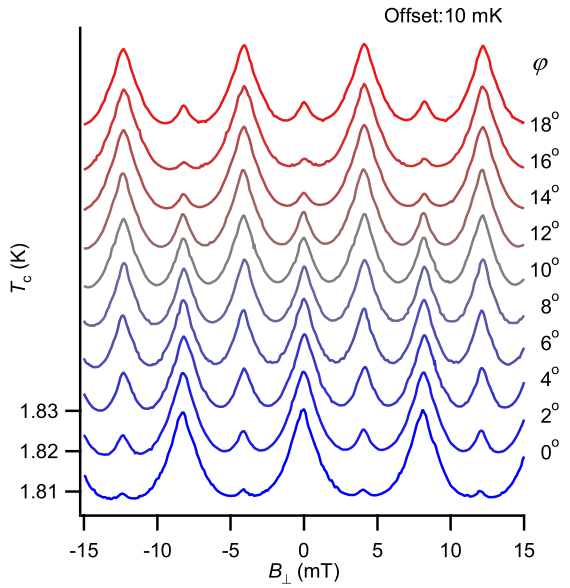

Fig. 2. (Color online) $T_{MF}(B)$ curves for different settings of φ and hence different values of β. Each trace is vertically offset by 10 mK for clarity. The period 8 mT of the LPO corresponds to one superconducting flux quantum per unit cell ($s = 500$ nm).

split coil magnet. Sample was directly immersed in superfluid helium and the temperature was stabilized to better than 2 mK by use of a suitable feedback circuitry. The current–voltage (I–V) curves were recorded by a dc current source and a voltmeter.

We fabricated and measured several SWN samples. They have given essentially the same results as the one presented in the next section. Sample-to-sample variations occurred with respect to the clarity of the fractional substructures which was attributable to small lithographic irregularity.

3. Experimental Results

3.1 Little–Parks oscillation

First, we fixed the temperature T near the mean field transition temperature T_{MF} and measured the resistance R of the SWN as a function of the perpendicular magnetic field B. The measurements were repeated at different temperatures and the results were then converted to $T_{MF}(B)$, by taking an arbitrary criterion that defined T_{MF} as a temperature at which $R(T, B) = 20\ \Omega \approx 0.3R_n$. The curves in Fig. 2 show the LPO of T_{MF} thus obtained. Adopting different resistance criteria does not affect the shape of LP oscillation. The different curves in Fig. 2 corresponds to different settings of φ and hence different values of β. The evolution of LPO with β reflects the corresponding evolution of the Hofstadter butterfly.[13] At $\varphi = 16°$, the peaks at half integer α become largest while those at integer α become smallest. In other words, the LPO pattern at $\varphi = 16°$ is shifted by a half cycle from that at $\varphi = 0°$. This indicates the condition $\beta = 1/2$ is realized at $\varphi = 16°$.

Figure 3 shows detailed comparison of the measured $T_{MF}(\alpha)$ (solid curves) with the spectral edge of Hofstadter butterfly (dotted curves). The only adjustable parameter is $\xi(0)$ in eq. (4). The fitting for each curve shown in Fig. 3 is obtained with the values of $\xi(0)$ falling in the range 60 ± 5 nm. This value is somewhat larger than the value

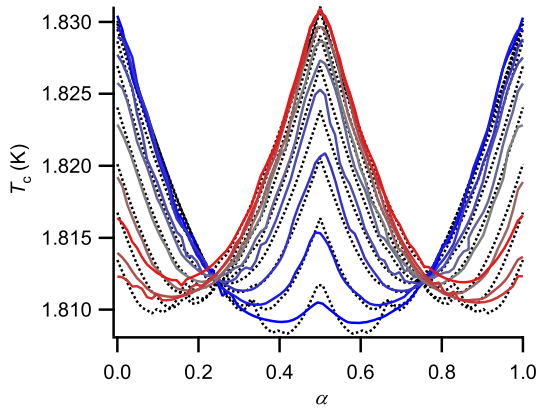

Fig. 3. (Color online) Comparison of LPOs between experiment and calculation. Colored solid curves are experimental and black dotted curves are calculated results. Each experimental curve corresponds to the same colored curve in Fig. 2.

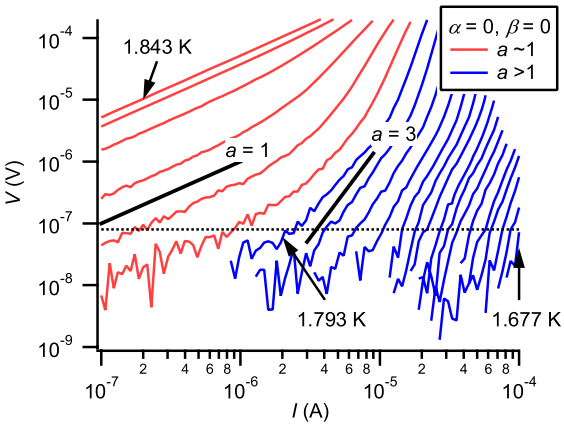

Fig. 4. (Color online) I–V characteristics at $\alpha = 0$ and $\beta = 0$. The data cover the temperature from 1.845 to 1.677 K in 8 mK steps. Critical temperature T_c is loosely defined as the temperature where the slope a starts to deviate from 1. Straight lines indicate slopes 1 and 3.

$\xi(0) \sim 34$ nm estimated from $H_{c2}(T)$ measurements. We note that the $\xi(0)$ extracted from eq. (4) depends on the resistance criterion and tends to decrease (approaches the estimate from H_{c2}) if we set it higher, i.e., closer to the normal resistance, than the one adopted here ($R = 20\ \Omega$). The result shown in Fig. 3 demonstrates that the checkerboard field with good uniformity and controllability is realized in this sample.

3.2 I–V characteristics

Measurement of the I–V characteristics is a useful tool to probe into the nature of superconducting transition, as it reveals the dissipation process associated with vortex dynamics.

3.2.1 $\beta = 0$

First, we focus on the case with no staggered magnetic field ($\beta = 0$). Figure 4 shows a log–log plot of the I–V characteristics around T_c, in the absence of the uniform and the modulated magnetic fields ($\alpha = \beta = 0$). Each I–V curve exhibits a power-law behavior $I \propto V^a$ for a certain range. Two straight lines drawn in the figure indicate slopes 1

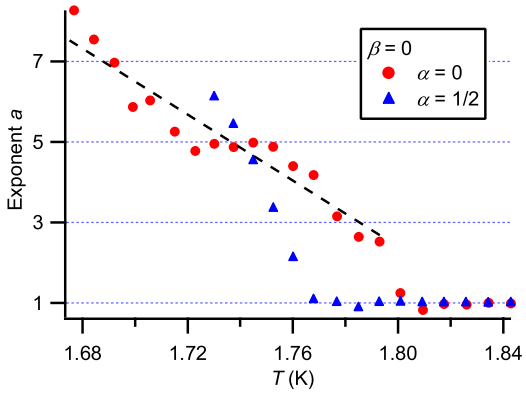

Fig. 5. (Color online) Temperature dependences of the power-law exponent a in the absence of modulated field ($\beta = 0$). Solid circles are the data for $\alpha = 0$. (The dashed line is guide to the eye). Triangles are the data for $\alpha = 1/2$.

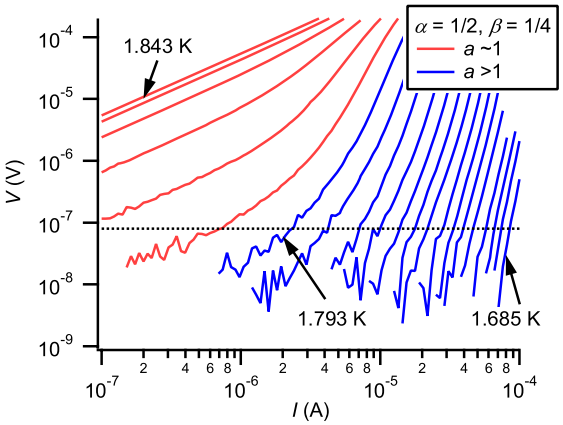

Fig. 7. (Color online) I–V characteristics at $\alpha = 1/2$ and $\beta = 1/4$. The temperature range is from 1.843 to 1.685 K in 8 mK steps. Critical temperature T_c is loosely defined as the temperature where the slope a starts to deviate from 1.

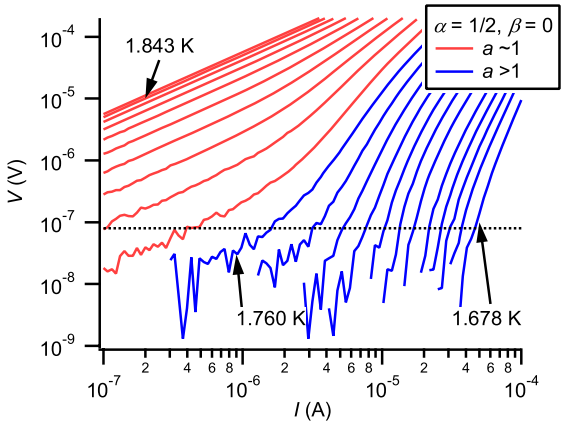

Fig. 6. (Color online) I–V characteristics at $\alpha = 1/2$ and $\beta = 0$. The temperature range is from 1.843 to 1.678 K in 8 mK steps. Critical temperature T_c is loosely defined as the temperature where the slope a starts to deviate from 1.

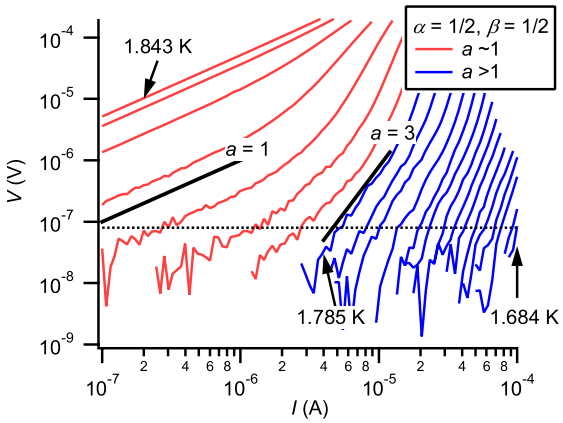

Fig. 8. (Color online) I–V characteristics at $\alpha = 1/2$ and $\beta = 1/2$. The temperature range is from 1.843 to 1.684 K in 8 mK steps. Critical temperature T_c is loosely defined as the temperature where the slope a starts to deviate from 1. Straight lines indicate slopes 1 and 3.

and 3. We extract the power-law exponent a from each I–V curve in the range around a voltage standard set at 8×10^{-8} V, which was chosen as low as possible while above the noise level by an appropriate margin. The temperature dependence of the exponent a thus obtained is plotted with solid circles in Fig. 5. As temperature is lowered, a jumps from 1 to ~3 at $T \sim 1.79$ K and then increases gradually. The behavior is consistent with the KTB transition.

Having confirmed that the transition at $\alpha = 0$ is consistent with the canonical KTB transition, we now turn to the fully frustrated case ($\alpha = 1/2$). The I–V characteristics for this case is shown in Fig. 6. In comparison with Fig. 4 for the $\alpha = 0$ case, first, the ohmic I–V behavior persists down to lower temperatures. T_c (loosely defined as the point where a starts to deviate from 1) is suppressed to ~1.76 K. Secondly, the slope of the I–V curve below and near T_c changes more rapidly. In addition, the negative curvature below T_c is more significant. Indeed, the power-law fitting failed for $T <$ 1.73 K. Since the values of a depend sensitively on the voltage criterion in this range, they are not reliable. Only the data for $T >$ 1.73 K are shown in Fig. 5. The suppression of T_c and the steeper increase of a below T_c for $\alpha = 1/2$ are similar to those reported by van Wees *et al.*[2] for their JJA sample.

3.2.2 $\beta \neq 0$

Next, we turn on the checkerboard magnetic field β and investigate its effect on the behavior for the fully frustrated case ($\alpha = 1/2$). Figures 7 and 8 show the I–V characteristics for $\beta = 1/4$ and $\beta = 1/2$, respectively. The suppression of T_c seen in $\alpha = 0$ and $\beta = 1/2$ is restored and the curves in $T < T_c$ are straight enough. As comparing the slope of the curve for the same temperature, the curves in Fig. 7 are steeper than the curves in Fig. 8. Figure 9 shows the evolution of the temperature dependence of a for $\alpha = 1/2$ with β changed from 0 to 1/2. As β is increased from zero, T_c increases rapidly and is recovered to the value in the absence of magnetic field (~1.8 K) for $1/4 < \beta < 1/2$. Concomitantly, the temperature dependence of a below and near T_c becomes less steep as β is increased from 0 to 1/2. It should be noted that the data for $\beta = 1/2$ are seemingly identical to those for the case of $\alpha = \beta = 0$. Namely, the canonical KTB transition is restored for this case.

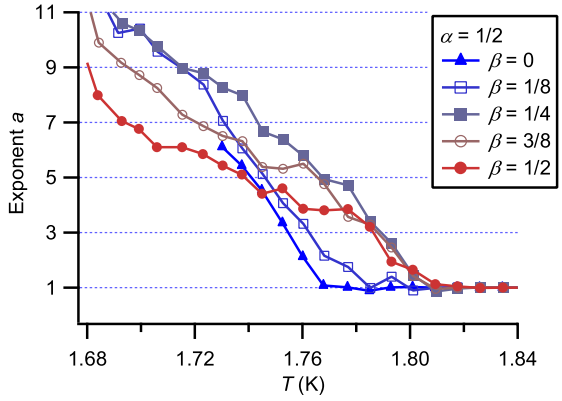

Fig. 9. (Color online) Temperature dependence of the power law exponent a of the I–V characteristics at $\alpha = 1/2$ for several values of β.

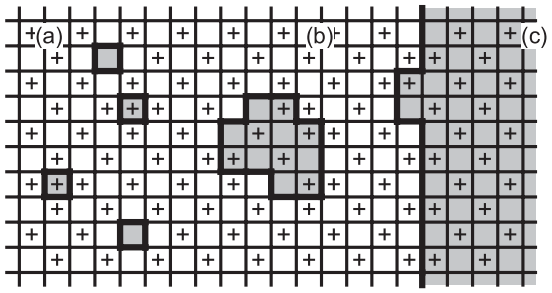

Fig. 10. Excitations in the FFXY model. (a) Vortex–antivortex pair. (b) Antiphase domain. (c) Kink–antikink pair on the domain wall.

4. Discussion

4.1 Review of theoretical studies on FFXY model

In order to understand the experimental findings given in the previous section, let us review some theoretical discussions on the FFXY model. As mentioned in the Introduction, this corresponds to the half-filled case ($\alpha = 1/2$) for the SWN, i.e., there exist half as many vortices as the plaquettes, and the vortices are expected to arrange themselves in a checkerboard pattern. The characteristic feature of the situation at $\alpha = 1/2$ as opposed to $\alpha = 0$ lies in that the ground state is doubly degenerate. The double degeneracy is due to the freedom of placing all vortices on black squares of a checkerboard, or on white ones. This leads to possible presence of anti-phase domains analogous to those in Ising spin systems. The FFXY system offers a simplest model case of competing XY and Ising ordering and has attracted much theoretical interest. Despite numerous studies on the FFXY and related models,[10,14–17] there seems much to be elucidated about the nature of phase transition in this class of systems.

The key ingredient is the interplay of the continuous XY symmetry and the discrete Ising symmetry. At finite temperatures, two types of thermal fluctuations, i.e., vortex pair excitation [Fig. 10(a)] and antiphase domain [Fig. 10(b)] can contribute to destruction of phase order. Two possible scenarios for the transition have been proposed. In one scenario, the XY and Ising order occur independently, so that there are two separate transitions, albeit very close to each other. The other scenario predicts that the interaction between XY-like and Ising-like excitations leads to a single transition, which belongs to a new universality class. Teitel and Jayaprakash[10] have shown that the temperature for vortex pair unbinding T_{KTB} cannot be higher than the Ising-like transition temperature T_{I} by domain wall proliferation.

Korshunov[18] emphasized the importance of kink–antikink pair excitation at an Ising-type domain boundary [Fig. 10(c)]. Dissociation of a kink–antikink pair is formally analogous to that of a vortex pair in the KTB transition. The KTB transition temperature T_{KTB} is given by the following condition.

$$k_{\mathrm{B}}T_{\mathrm{KTB}} = \frac{\pi}{2}\Gamma(T_{\mathrm{KTB}}), \tag{5}$$

where $\Gamma(T)$ is the helicity modulus, which is the quantity representing the system's rigidity against phase twist of the order parameter. Γ is a decreasing function of T because increase of thermal fluctuation causes the reduction of phase stiffness. The above formula implies that when Γ decreases to a value equal to $(2/\pi)k_{\mathrm{B}}T$, nucleation of free vortices becomes favored by the entropy term. As the free vortices further destroy the phase correlation, $\Gamma(T)$ exhibits sudden drop from $(2/\pi)k_{\mathrm{B}}T$ to 0. Because the I–V exponent a is directly related to Γ as

$$a(T) = 1 + \frac{\pi\Gamma(T)}{k_{\mathrm{B}}T}, \tag{6}$$

this sudden drop leads to the jump in a from 3 to 1. This is called universal jump.

The temperature T_{kink} for kink–antikink unbinding at the Ising antiphase boundary is given by a similar expression.

$$k_{\mathrm{B}}T_{\mathrm{kink}} = \frac{\pi}{4}\Gamma(T_{\mathrm{kink}}). \tag{7}$$

The difference of the numerical factor between eqs. (5) and (7) is traced to the fact that the net charge of kink and antikink are $\pm 1/2$ and that they occur on the one-dimensional Ising domain boundary. Figure 11 shows schematic temperature dependence of Γ and the conditions corresponding to eqs. (5) and (7). It can be readily seen that eq. (7) gives a transition temperature slightly lower than the T_{KTB}.

Free kinks (and antikinks) on a domain boundary destroy the phase correlation across the boundary. Below T_{kink}, there

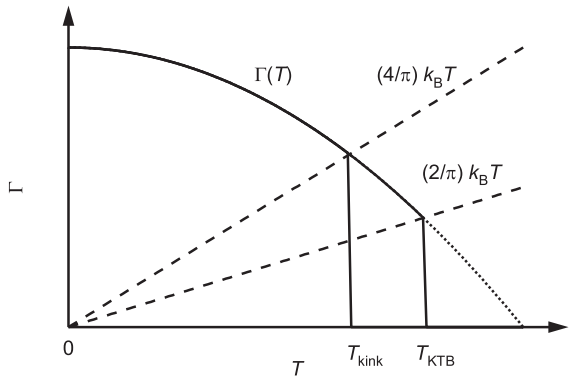

Fig. 11. Schematic temperature dependence of Γ. The temperatures where the curve of Γ crosses the upper and lower dashed line give T_{kink} and T_{KTB}, respectively.

is no free kink on the boundary and the global phase order is preserved even in the presence of the Ising domains. The phase correlation across the domain boundaries is effectively destroyed above T_{kink} where there are many free kinks on the domain boundaries. The destruction of phase correlation across the domain boundary due to kink–antikink unbinding results in a sudden drop of the phase stiffness, so that vortex pair unbinding takes place concomitantly. In other words, the kink–antikink unbinding transition triggers a "KTB-like" transition with a jump of helicity modulus significantly larger than the universal jump for the canonical KTB transition, as seen from Fig. 11. The KTB-like transition predicted in this scenario occurs at a different (lower) temperature than that for the Ising transition because the kink–antikink unbinding can occur without proliferation of domain boundary. In this sense it supports the scenario of two separate transitions. The above picture first proposed by Korshnov[18] has been subsequently supported by numerical simulation studies.[19,20]

4.2 *Interpretation of the experimental results*

Let us now return to the present experiment and see if the experimental results can be interpreted in the light of above models. We can summarize the salient features of our experimental data as follows:

First, with regard to the transition of fully frustrated ($\alpha = 1/2$) case in the absence of the field modulation ($\beta = 0$);

(1) T_{c} is suppressed in comparison to the canonical KTB transition for $\alpha = 0$ and the temperature dependence of a below and near T_{c} becomes steeper.

Secondly, with regard to the effects of the checkerboard field on the transition at $\alpha = 1/2$;

(2) As β is increased from 0 to 1/4,
- The suppression of T_{c} is recovered rather quickly.
- The temperature dependence of a below and near T_{c} become less steep.

(3) In the range $1/4 \leq \beta \leq 1/2$,
- T_{c} is not changed so much.
- The temperature dependence of a below T_{c} becomes smaller as β is increased.

(4) At $\beta = 1/2$,
- The behavior of a is identical to that of KTB transition for $\alpha = \beta = 0$ case.

The feature (1) is naturally explained by the kink–antikink dissociation scenario. This scenario predicted the larger jump in helicity modulus Γ than the canonical KTB transition. As shown in Fig. 11, this jump should occur at T_{kink} which is slightly lower than T_{KTB}. The experimental observation of steep drop of a as T_{c} is approached from below conforms with this picture.

The feature (2) refers to the effect of β on the phase transition at $\alpha = 1/2$. As stated earlier, the checkerboard field plays the role of lifting the double degeneracy of vortex configuration. The observed trend can be understood by considering how antiphase domains are affected by β. With increasing β, the antiphase domains become more and more costly, so that they will be smaller in size and distributed more sparsely. Because kinks and antikinks occur only on domain boundaries, their destructive effect on the phase order is limited to the peripheries of the antiphase domains. This local phase disordering would disturb the global phase order *only when* the antiphase domains are relatively dense. In other words, the scenario of the kink-pair-unbinding-induced "KTB-like" transition is valid only if the mean separation D between antiphase domains is not too large, which is the case for small values of β. With increasing β, antiphase domains becomes more sparsely distributed (D becomes larger) so that the effect of the local phase disordering by the free kinks at the domain boundaries becomes less effective in disturbing the global phase order. There should be a certain critical value for D above which the kink transition becomes irrelevant to the destruction of global phase order. From the data shown in Fig. 9, this crossover seems to occur somewhere between $\beta = 1/8$ and $1/4$.

Although the scenario we presented above can explain the feature (2), this simple scenario fails to explain the feature (3). According to the above scenario, the phase rigidity is never enhanced as compared with the case without the antiphase domain. Therefore the exponent a which is related to the helicity modulus is not expected to exceed the value for the $\alpha = \beta = 0$ case, in disagreement with the experimental finding. This discrepancy may be resolved at least partially by considering the KTB-type vortex pair unbinding in the presence of antiphase domains. The above scenario is too simplistic in neglecting the interaction between vortices and antiphase domains. In actuality, if a vortex comes close to an antiphase domain, it tends to merge with the domain. Let us consider a situation that the bulk of the system is predominantly single domain with sparse patches of antiphase domains, with mean separation D. Only vortex pairs smaller than D survive, since larger ones are "absorbed" by the antiphase domains. Since the I–V characteristics reflects the current-induced unbinding of the vortex pairs with different size (and hence different binding energy), the extinction of vortex pairs larger than D should affect the I–V characteristics. Thus the presence of antiphase domains changes the I–V exponent by partially suppressing the thermal excitation of vortex pairs. Loosely speaking, the presence of antiphase domains is similar in effect with a lower effective temperature so that it results in larger values of the exponent a. For $\alpha = 1/2$ and $\beta = 1/2$, the system consists purely of single domain and the KTB transition due to vortex-antivortex unbinding is observed. As β is reduced from $1/2$, patches of small antiphase domains emerge and they act to enhance the exponent a below T_{c} by the above mechanism. This qualitatively explains the trend of a below T_{c} for $1/2 \geq \beta \geq 1/4$ seen in Fig. 9. For $\beta < 1/4$, free kinks are more effective for phase disordering than vortices so that the behavior of the exponent a can be described by kink–antikink unbinding scenario.

5. Conclusion

In conclusion, the superconducting transition of SWN under uniform and modulated magnetic fields is studied by the measurement of I–V characteristics. Transition at zero magnetic field ($\alpha = \beta = 0$) is the KTB type with a jump of the power-law exponent a from 1 to 3. The fully frustrated case ($\alpha = 1/2$ and $\beta = 0$) exhibits a "KTB-like" transition with a jump of a larger than the universal value, which is consistent with a picture that the transition is triggered by

kink–antikink unbinding at antiphase domain boundaries. Application of a checkerboard field lifts the double degeneracy inherent to the system at $\alpha = 1/2$. The nature of transition at $\alpha = 1/2$ is altered by increasing β from 0 to $1/2$, until the canonical KTB transition is restored at $\beta = 1/2$. A key parameter governing the nature of phase transition is the mean separation D between antiphase domains. For smaller values of β, the antiphase domains are relatively dense (D is sufficiently small) in the phase transition regime, so that the kink–antikink unbinding scenario is an appropriate description of the transition. For larger values of β, free kinks at the domain boundaries are no longer effective in disturbing the global phase order. The behavior of a in this regime can be qualitatively explained by considering vortex-antivortex pair excitation in the presence of sparse patches of antiphase domains.

Acknowledgment

This work is supported in part by a Grant-in-Aid for Scientific Research from the Ministry of Education, Culture, Sports, Science and Technology (MEXT) of Japan, and also partly supported by Special Coordination Funds for Promoting Science and Technology.

1) R. S. Newrock, C. J. Lobb, U. Geigenmueller, and M. Octavio: in *Solid State Physics*, ed. H. Ehrenreich and F. Spaepen (Elsevier, Amsterdam, 1999) Vol. 54, p. 263.
2) B. J. van Wees, H. S. J. van der Zant, and J. E. Mooij: Phys. Rev. B **35** (1987) 7291.
3) H. S. J. van der Zant, M. N. Webster, J. Romijn, and J. E. Mooij: Phys. Rev. B **50** (1994) 340.
4) S. Alexander: Phys. Rev. B **27** (1983) 1541.
5) M. Tinkham, D. W. Abraham, and C. J. Lobb: Phys. Rev. B **28** (1983) 6578.
6) B. Pannetier, J. Chaussy, R. Rammal, and J. C. Villegier: Phys. Rev. Lett. **53** (1984) 1845.
7) D. R. Hofstadter: Phys. Rev. B **14** (1976) 2239.
8) F. Yu, N. E. Israeloff, and A. M. Goldman: Phys. Rev. Lett. **68** (1992) 2535.
9) X. S. Ling, H. J. Lezec, M. J. Higgins, J. S. Tsai, J. Fujita, H. Numata, Y. Nakamura, Y. Ochiai, C. Tang, P. M. Chaikin, and S. Bhattacharya: Phys. Rev. Lett. **76** (1996) 2989.
10) S. Teitel and C. Jayaprakash: Phys. Rev. B **27** (1983) 598.
11) S. Ito, M. Ando, S. Katsumoto, and Y. Iye: J. Phys. Soc. Jpn. **68** (1999) 3158.
12) M. Ando, S. Ito, S. Katsumoto, and Y. Iye: J. Phys. Soc. Jpn. **68** (1999) 3462.
13) Y. Iye, E. Kuramochi, M. Hara, A. Endo, and S. Katsumoto: Phys. Rev. B **70** (2004) 144524.
14) E. Granato, J. M. Kosterlitz, J. Lee, and M. P. Nightingale: Phys. Rev. Lett. **66** (1991) 1090.
15) J. R. Lee: Phys. Rev. B **49** (1994) 3317.
16) G. Ramirez-Santiago and J. V. Jose: Phys. Rev. B **49** (1994) 9567.
17) Y. M. M. Knops, B. Neinhuis, H. J. F. Knops, and H. W. J. Bloete: Phys. Rev. B **50** (1994) 1061.
18) S. E. Korshunov: Phys. Rev. Lett. **88** (2002) 167007.
19) P. Olsson and S. Teitel: Phys. Rev. B **71** (2005) 104423.
20) M. Hasenbusch, A. Pelissetto, and E. Vicari: Phys. Rev. B **72** (2005) 184502.